Applied Catalysis B: Environmental 306 (2022) 121105

Contents lists available at ScienceDirect

Applied Catalysis B: Environmental

journal homepage: www.elsevier.com/locate/apcatb

Biologically bound nickel as a sustainable catalyst for the selective hydrogenation of cinnamaldehyde

Parul Johar [a], C. Robert McElroy [a], Elizabeth L. Rylott [b], Avtar S. Matharu [a], James H. Clark [a,*]

[a] Green Chemistry Centre of Excellence, Department of Chemistry, University of York, York YO10 5DD, UK
[b] Centre for Novel Agricultural Products, Department of Biology, University of York, Wentworth Way, York YO10 5DD, UK

ARTICLE INFO

Keywords:
Metal bio-refinery
Bio-catalysis
Microwave assisted pyrolysis
Selective hydrogenation
Sustainable chemical production

ABSTRACT

With mounting concerns over critical element sustainability in future bio-refineries, the conversion of phyto-extracted nickel (from contaminated lands) into an inexpensive and clean catalyst could help to reduce demand for virgin precious metals. Utilizing this green approach, noble metal catalysts, which require substantial downstream processing, could potentially be replaced by a naturally developed non-noble metal catalyst. We report a biologically bound non-noble metal catalyst (Ni-phytocat, 0.1–2.5 wt% Ni) prepared using simple, one-step, energy efficient, microwave-assisted pyrolysis (250℃, 200 W, <10 min). The biologically bound Ni in the plant matrix directs the catalytic hydrogenation of cinnamaldehyde selectively and efficiently (up to 97% conversion and 96% selectivity at T≤*120* ℃), Our findings indicate that the presence of bio-carbon matrix around the phyto-extracted Ni enables an efficient suppression of the over-hydrogenation reaction pathway and prevents further dissociation of adsorbed hydrocinnamaldehyde molecules. The simplicity, long-term stability and ease of handling make this catalyst an economically and environmentally attractive alternative to Raney nickel and precious metal–based catalysts.

1. Introduction

Globally, mining influences 5000 Mha of land surface, with 7% overlapping with key biodiversity areas and 8% with protected areas [1]. Most mining regions (∼ 81%) target metals such as copper, nickel, and lithium needed for renewable energy production [1]. Identified land-based resources contain at least 0.3 billion tons of nickel (Ni), with about 60% in laterites and 40% in sulfide deposits [2]. Because of its widespread usage and tendency to accumulate, Ni contamination has reached above its ecological threshold, accounting for approximately 5% (8.75 Mha) of E.U. agricultural land area [3]. The metal contamination in agricultural soils is an obstruction to achieving global food safety and security and will worsen as climate change reduces crop yields. Phyto-remediation is a promising nature-based solution for treating the contamination; however, several issues must be addressed before it can be broadly implemented [4,5]. Firstly, plant selection is a critical step; although hyper-accumulators are able to extract large amounts from the contaminated land (up to 1000 mg kg^{-1} dry tissue), they might not be suitable for soils contaminated with multiple contaminants [4,5]. In these cases, fast-growing and high-biomass yielding plants including willow (*Salix viminalis*) or poplar trees can be used to extract a wide range of metals from soil [6]. Secondly, the harvested biomass is typically incinerated, leaving behind a metal-concentrated bottom ash usually disposed of in landfills. However, harvested biomass can be used as a feedstock for production of bio-energy or bio-materials [7–10].

Over the past few years, the development of catalytically active materials derived from biomass has attracted huge attention, owing to their unique qualities of widespread availability, natural abundance and renewability, and relatively low-cost [8,9,11–13]. To date, several synthetic procedures have been reported for fabricating bio-catalysts including wet impregnation, ion-exchange, co-precipitation, reduction, high-temperature pyrolysis, atomic layer deposition and so on [8,11,14,15]. However, these protocols focus on artificial incorporation of noble and non-noble metallic species onto bio-derived carbon materials [11–16]. There is now interest in developing biocatalysts from plants that have taken up nickel through natural, biological processes. This process allows both the recapturing of a limited, natural resource, remediation of land, and once the catalyst is used-up, the metal can be reused, presenting a sustainable, circularity. In this context, we envisioned the development of our phytocat materials, prepared using a simple, one-step protocol using plant biomass rich in nickel accumulated

* Corresponding author.
E-mail address: james.clark@york.ac.uk (J.H. Clark).

https://doi.org/10.1016/j.apcatb.2022.121105
Received 11 October 2021; Received in revised form 13 December 2021; Accepted 14 January 2022
Available online 19 January 2022
0926-3373/© 2022 Elsevier B.V. All rights reserved.

by the plant during growth on nickel contaminated wastelands. There has been progress in development of efficient non-noble metal catalysts derived from various biomass feedstocks for green and sustainable selective hydrogenation transformations [8,14,15]. Non-noble metals, such as nickel (Ni) offer appealing attributes that address the disadvantages of precious metals, including platinum (Pt), palladium (Pd) and ruthenium (Ru) i.e. high cost, low abundance, and toxicity [17,18]. At an industrial level, hydrogenations are usually performed with these noble metals or base metal catalysts, such as Raney nickel [19,20]. Despite the high activity and low cost of Raney nickel, this catalyst is often sensitive and non-selective due to large metal surface area, making it pyrophoric and leading to difficulties in handling [20,21]. As a consequence, there is an industrial and academic need for the development of an inexpensive, safe and stable alternative to Raney nickel which should be easy to handle as well as more selective towards functional molecules. Consequently, in recent years, significant efforts have been made to develop alternative Ni-based hydrogenation catalysts [14,16,22,23].

Cinnamaldehyde (CAL) represents a typical model compound of the coniferyl aldehydes derived from lignin [24]. It can be produced by electron abstraction of the phenoxy radicals followed by disruption of the Cα-Cβ bond through retro-aldol cleavage of lignin [24]. Lignin-derived chemicals can serve as platform molecules for the production of a wide range of value-added chemicals, with implementation motivating the transformation towards a sustainable chemical industry. Chemoselective hydrogenation of C═C and, or C═O in b,h-unsaturated aldehydes is an indispensable approach in fine chemical manufacturing. Cinnamaldehyde is an industrially important molecule, because its partial hydrogenation products, i.e. cinnamyl alcohol (COL) and hydrocinnamaldehyde (HCAL) are key intermediates for the synthesis of high-value products, including perfumes, flavorings and pharmaceuticals [25–28]. The production of saturated aldehydes from unsaturated ones has also industrial and biological applications. For example, hydrocinnamaldehyde derived from cinnamaldehyde hydrogenation can be used in the synthesis of an intermediate reagent of anti-viral pharmaceuticals, particularly HIV protease inhibitors [29]. At present, the major pathway of HCAL synthesis is the toluene chlorination-hydrolysis method [26]. Another method for the synthesis of HCAL and its derivatives (11–67% yield) is through a five-step process from the Knoevenagel condensation of aldehydes with Meldrum's acid [30]. Moreover, Frost et al. reported the hydrosilylation of Meldrum's acid by a multi-step process, using palladium or molybdenum catalysts [31,32]. Instead of these complex multi-step processes, selective hydrogenation of CAL to a HCAL reaction does not produce any corrosive byproduct or toxic waste [14,15,25,26]. Most of the accomplished work on the partial reduction of cinnamaldehyde reported either poor selectivity (<13%) or poor conversion (<63%) [33–35]. Moreover, there remain challenges associated with the overall sustainability of the transformation i.e. relatively high cost or complex synthetic protocol for catalyst preparation or high reaction temperatures (T > 150℃) [33–35]. Herein, we report an air-stable, inexpensive and highly selective, biologically bound Ni catalyst (phytocat) that can be used for hydrogenation transformations. One of the major obstacles that hinders progress in this important area of catalysis is the difficulty of catalyst preparation [26]. The simple, one-step, low- temperature, microwave biosynthesis of the novel catalyst presented here make it an attractive alternative to current hydrogenation catalysts, which are typically fabricated via multi-step synthesis. Our Ni-based biocatalyst represents a hybrid platform consisting of naturally occurring, inorganic components with lignocellulose providing an exciting opportunity to advance green chemistry applications. The biologically bound Ni in the plant matrix directs the catalytic hydrogenation of cinnamaldehyde, thereby avoiding multi-step processes and the need for traditionally mined metal.

2. Experimental

2.1. Materials and chemicals

Two varieties of biomass were used in our experiments, the Ni hyperaccumulator (*Alyssum murale*, collected from field on nickel-rich soils) and hydroponically-grown willow plant species for the preparation of phyto-catalyst (2.5 wt% and 0.1 wt% Ni respectively) and Ni free controls (<0.01 wt% Ni). Metal accumulation was determined in leaves and stems using an inductively coupled plasma optical emission spectrometer (ICP-OES, Agilent 700 series) (Table S1). All other chemicals were purchased from Sigma-Aldrich and were used as received unless otherwise stated.

2.2. Catalyst preparation

The catalyst was prepared using the method described previously [36]. Briefly, microwave assisted pyrolysis on air-dried, ground leaf tissues from the plant species was performed on a CEM Discover, equipped with 10 mL quartz vial under N_2 at 250 °C and 200 W to produce bio-char with different Ni-loadings (termed as phytocat). The feedstock was converted into vapors, which were passed through a condenser and collected as liquid oil. The mass yield of bio-char and bio-oil produced were measured and the gas yield calculated as the mass balance of the original sample. The total conversion was evaluated based on the sum total of liquid and gas yields. After the successful extraction of bio-oil and bio-gas, the bio-char containing naturally bound nickel with different metallic loadings was used as catalyst.

2.3. Catalyst characterization

High-angle annular dark-field -scanning transmission electron microscope (HAADF-AC-STEM) images were acquired using a 200 keV JEOL 2200FS scanning transmission electron microscope with a field emission gun. Transmission electron microscopy (TEM, JEOL 2010) was used under the accelerating voltage of 200 kV. Microstructural and chemical information of phytocat was obtained by using a field-emission scanning electron microscope (FE-SEM) equipped with an energy-dispersive X-ray (EDX) spectrometer (JSM-7800 F PRIME, JEOL Ltd.). Elemental composition and valence near the surface were measured using XPS (AXIS Ultra DLD, Kratos. Inc.). XRD was performed at operating voltage of 40 kV, current, 40 mA, scan speed of 0.1 s/step and the scan scope from 10 Θ to 90 Θ using a Bruker AXS D8 Advance. Further, Ni particle size was estimated using the Scherrer equation using the peak centered at $2\theta = 44.5^{\circ}$. N_2 adsorption–desorption analysis was performed at 77 K using a TriStar (Micromeritics Instrument Corp.; Norcross, GA, USA), equipped with automated surface area and pore size analyser. Before analysis, samples were degassed at 180 °C for 4 h Fig. S6). The detailed procedures are described in SI.

2.4. General procedure for hydrogenation

The liquid-phase CAL hydrogenation was tested in a stainless steel multipoint (6 × 10 mL pots) reactor (manufactured at chemistry workshops, University of York). For a typical test, cinnamaldehyde (1 mmol), anisole (internal standard, 0.5 mmol), 10–50 mg of catalyst (0.01–0.08 mmol Ni) and iso-propanol (solvent, 5 mL) were loaded into the reactor. The reaction was conducted with stirring (250 rpm) at 60–120 °C. The reaction was stopped after a proper time (1–24 h) and the products were analyzed using a GC (GC-2014, Shimadzu) equipped with a flame ionization detector (FID) and GC–MS (JEOL AccuTOF-GCx plus, Agilent 7890B GC). After completion of the reaction, the solvent was removed under reduced pressure at 45 °C. The products were analyzed by ^{1}H NMR and ^{13}C NMR spectroscopy in $CDCl_3$ (Fig. S16-21) and FT-IR analysis (Fig. S9-15). The used catalysts were easily recovered, washed using iso-propanol and dried for 24 h. The recyclability

tests were performed using the recovered catalysts to test their stability. The detailed procedures are described in SI.

$$\text{CAL conversion}(\%) = \frac{\text{moles of CAL before reaction} - \text{moles of CAL after reaction}}{\text{moles of CAL before reaction}} \times 100\% \quad (1)$$

$$\text{Product selectivity}\ (\%) = \frac{\text{moles of product}}{\text{moles of CAL consumed}} \times 100\% \quad (2)$$

3. Results and discussion

3.1. Formation and structural characterization of naturally entrapped nickel in the phytocat

Salix vimnalis (willow) and the Ni hyper-accumulating plant *Alyssum murale* were used in this study. The Salix species contain a genetically diverse range of phenotypes, include broad variation in the ability to withstand Ni tolerance, and rate of Ni uptake. This variation offers the opportunity to use breeding to improve the desired Ni tolerance and uptake traits. Using willow has the advantages that it is a high biomass crop that grows vigorously in a broad range of environmental conditions and geographical locations, and is farmed using existing agricultural infrastructure [6]. The amount of Ni present within the biomass of each plant is determined by the biology of that species (including the gene-encoded metal transporters and associated detoxification enzymes) [4–6]. Six-week old, hydroponically-grown *S. vimnalis* rods were dosed with 100 mg kg^{-1} Ni for two weeks, the tissues air-dried and ground. *Alyssum murale* was grown in Ni-rich soil. The nickel catalysts were prepared using the ground plant materials in one- step, low temperature, microwave-assisted pyrolysis (200 W, 250 °C) to produce *S. viminalis* bio-char (0.1 wt% Ni, termed Ni-phytocat-0.1), and *A. murale* bio-char (2.5 wt% Ni, termed Ni-phytocat-2.5) [36]. The control catalyst was prepared using *S. viminalis* bio-char that had not been dosed with Ni (<0.01 wt% Ni, termed as control phytocat). Phytocat as a good microwave absorber, aids in transferring the microwave energy leading to the in-situ synthesis of catalytically active Ni^0 from phyto-accumulated Ni^{2+} (Fig. 1a) [37].

Field emission scanning electron microscopy (FESEM) images of phytocat materials exhibit irregular spherical morphologies and high dispersion of Ni species on the surface of Ni-phytocat-2.5 (Fig. 1c-d) and relatively moderate dispersion on Ni-phytocat-0.1 (Fig. 1e-f). But the presence of Ni wasn't detected on the surface of irregular clusters of control phytocat (Fig. 1g-h). Energy-dispersive x-ray (EDX) spectroscopy analysis of the nickel phytocat reveals the presence of small amounts of oxygen, which is evident of nickel oxide formation on the particle surface due to storage in air. As can be seen from Fig. 2a-b, nickel nanoparticles embedded in a bio-carbon matrix of phytocat contained traces of calcium, silicon and oxygen.

Following the microstructural features, high-angle annular dark-field scanning transmission electron microscopy (HAADF-STEM) images demonstrate the morphology of the catalysts. In the field of view of HAADF-STEM images, intensity is relative to the square of atomic number of the element [38]. Therefore, the atomically dispersed Ni particles can be clearly distinguished as the brighter spots on bio-carbon. As shown in Fig. 2c, the formed Ni nanoparticles are uniformly

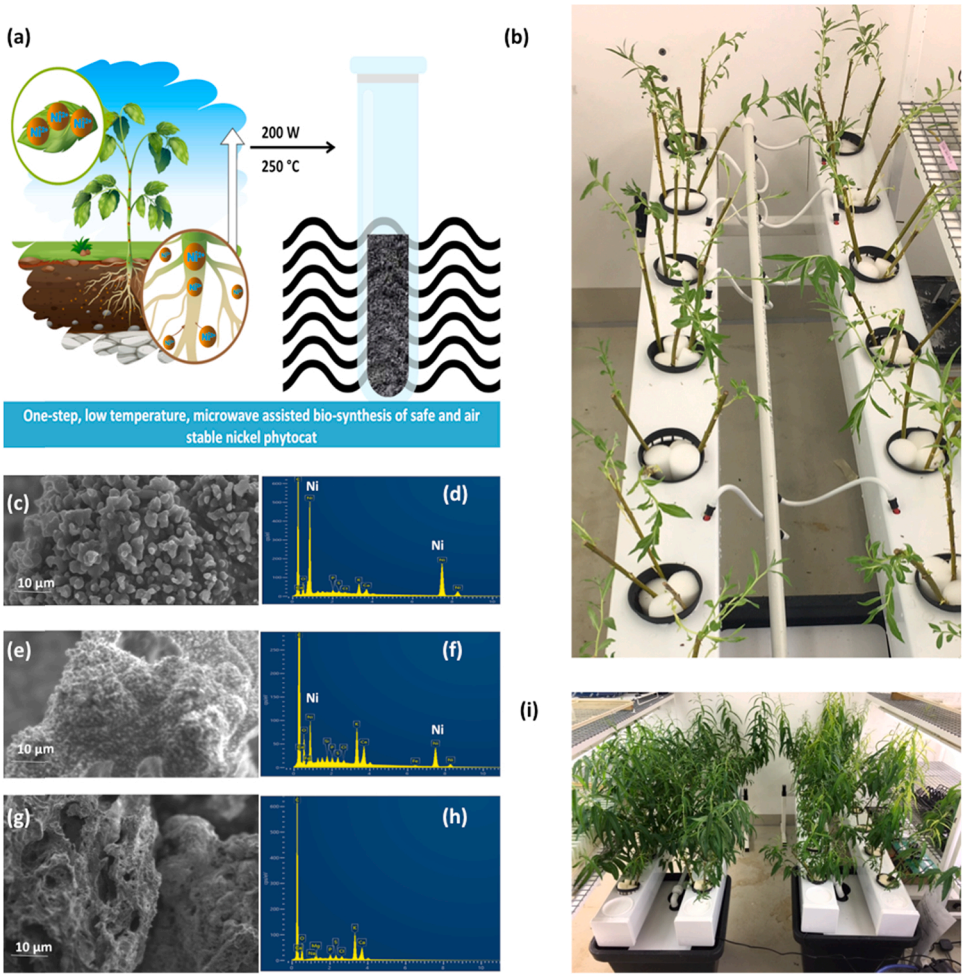

Fig. 1. (a) Formation of naturally entrapped nickel catalyst (phytocat) using low temperature microwave assisted pyrolysis of nickel contaminated plant biomass, (b) Aeroflo system (General Hydroponics) used to grow willow rods (*Salix viminalis*, 6 weeks duration) for preparation of phytocat-0.1 and control phytocat, Scanning electron microscopy (SEM) images equipped with energy-dispersive X-ray spectroscopy (EDX) (c-d) phytocat-2.5, (e-f) phytocat-0.1 and (g-h) control phytocat, (i) nickel dosed willow rods (100 mg kg^{-1}, 2 weeks duration) for preparation of phytocat-0.1.

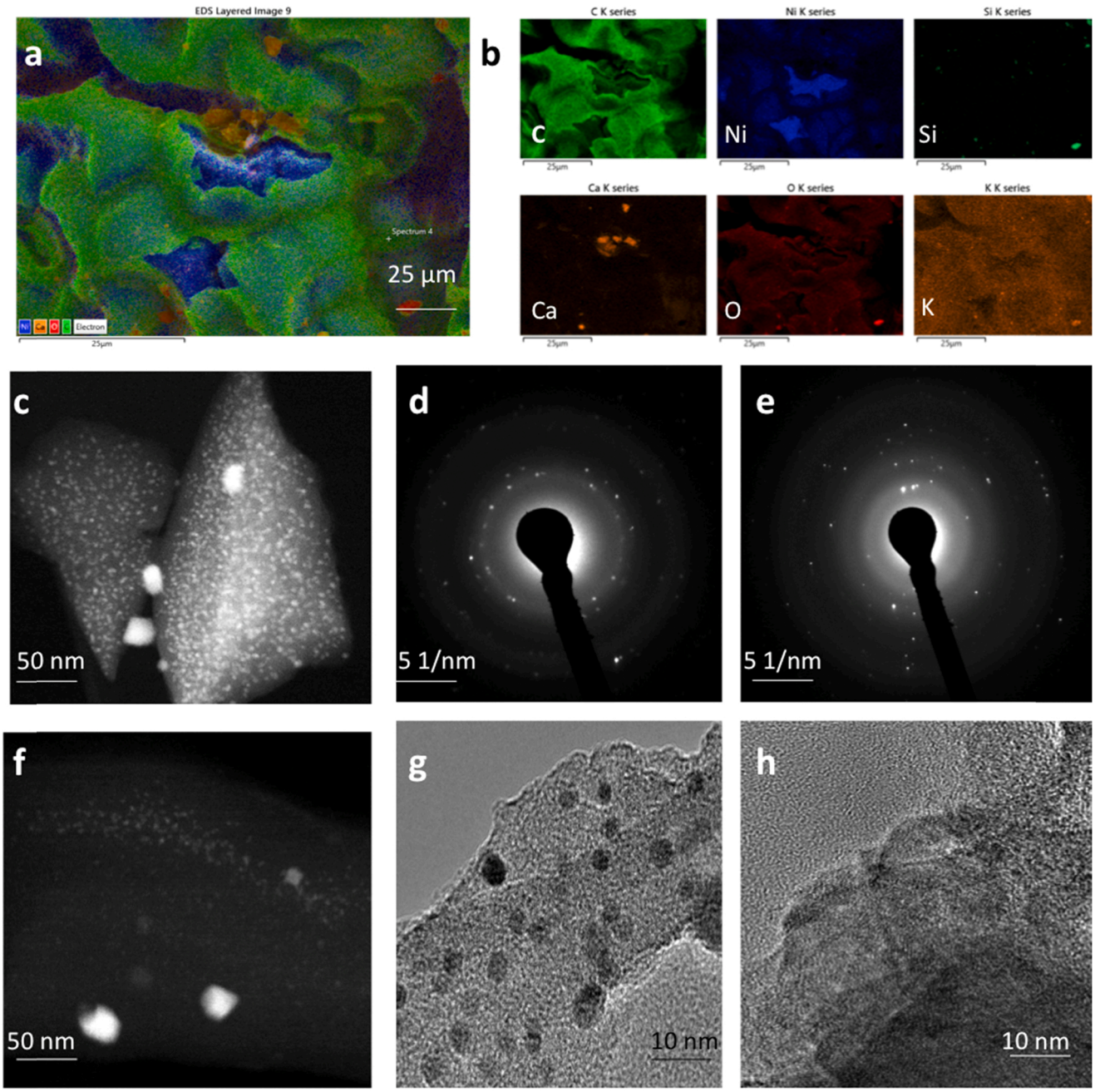

Fig. 2. (a) Energy-dispersive x-ray (EDX) spectroscopy analysis of Ni-phytocat-2.5 highlighting carbon (green), nickel (blue), oxygen (red) and calcium (orange), (b) Elemental mapping of Ni-phytocat-2.5 highlighting carbon, nickel, silicon, calcium, potassium and oxygen, (c, f) high-angle annular dark-field scanning transmission electron microscopy (HAADF-STEM) image of Ni-phytocat-2.5 and Ni-phytocat-0.1 respectively, (d-e) selected-area electron diffraction (SAED) patterns of Ni phytocat-2.5 before and after catalytic hydrogenation of cinnamaldehyde, (g-h) high-resolution TEM (HRTEM) image of Ni-phytocat-2.5 and Ni-phytocat-0.1 respectively.

distributed and exhibit an average particle size of 5.2 ± 1.1 nanometers. Most of the observed nano-particles were within a range of 4.5–7.3 nm; however, a few particles up to 11 nm were observed. STEM analysis of phytocat material revealed metallic Ni nanoparticles with thin oxidic shells.

After use, the recycled catalysts have a more compact structure, with Ni nano-particles embedded in amorphous bio-carbon (Fig. S1a, c). The brighter contrast in the HAADF STEM image (Fig. S1a) shows very little rearrangement of Ni on the surface. These Ni NPs contained within the bio-carbon matrix of phytocat possess good thermal stability because of the constraint of the carbon support, which limits its aggregation and leads to excellent catalytic activity [38].

The selected-area electron diffraction (SAED) patterns of Ni phytocat, shown in Fig. 2d-e, reveals the polycrystalline nature and different crystal faces of naturally entrapped Ni on bio-carbon. The diffraction rings are allocated to (111), (200), and (220) planes and in good agreement with XRD results (Fig.3e-f).

Intrigued by these characteristics, we performed high-resolution transmission electron microscopy (HR-TEM) measurement to observe the lattice fringes corresponding to the naturally entrapped nickel in the phytocat materials. The high-resolution TEM (HRTEM) image (Fig. 2g-h) reveals some irregular fringes, mainly with a planar spacing of 0.242 nm and 0.216 nm point to (111) and (200) crystal planes, respectively, of cubic Ni phase [39].

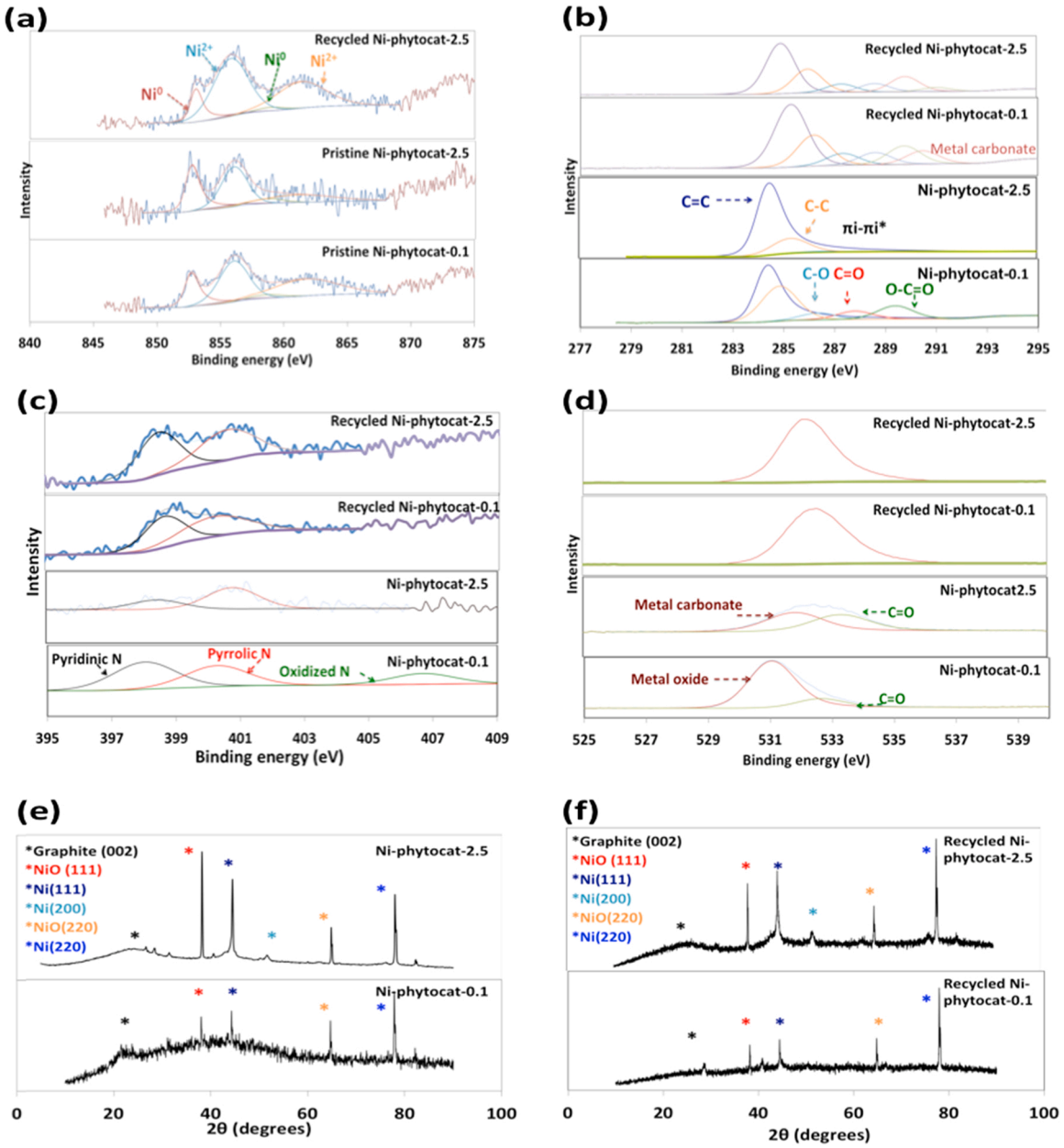

Fig. 3. X-ray photoelectron spectroscopy (XPS) analysis of phytocat materials (a) deconvoluted high-resolution Ni2p$_{3/2}$ spectra (b) deconvoluted high-resolution N 1s XPS spectra, (c) deconvoluted high-resolution C 1s spectra, (d) deconvoluted high-resolution O 1s spectra, (e) X-ray diffraction (XRD) pattern of Ni-phytocat-2.5 and −0.1, (f) XRD pattern of recycled Ni-phytocat-2.5 and −0.1.

The elemental composition and chemical states of naturally bound nickel in the bio-carbon matrix were analyzed by X-ray photoelectron spectroscopy (XPS) analysis.

Various plant based ligands like histidine, nicotianamine and various organic acids form complexes with Ni^{2+} ions, enabling its uptake by plants [37]. Our one-step, low temperature microwave assisted pyrolysis approach leads to in-situ formation of Ni^0. This chemical valence state of the naturally entrapped Ni was determined using the corresponding binding energies (eV) of Ni2p$_{3/2}$ peaks, as shown in Fig. 3a. Generally, catalysts with low nickel metallic loadings are dominated by Ni^{2+} along with some sequestered Ni^0 sites [40]. The differences in metallic nickel leads to changes in the surface chemistry and consequently the catalytic activity [40]. However, an oxide layer formed around supported Ni particles can suppress coke formation while preserving high catalytic activity [40]. The peak around 852 eV is assigned to Ni^0 and peaks between 855 and 861 eV are assigned to Ni^{+2} in the form of Ni(OH)$_2$ and NiO.[2] The surface of the phytocat consisted of both Ni^0 and Ni^{2+}. However, with increasing nickel content, there is an increase in intensity of Ni^0 peak with a simultaneous decrease in intensity of Ni^{+2} peak. After use, the recycled catalyst was analyzed and found to have a slight decrease in the intensity of the Ni^0 peak. Taking into consideration that these valence states only belong to the outer layers of the phytocat, these results suggest the formation of a unique structure where a pure nickel core is surrounded by a shell of NiO and Ni(OH)$_2$.

Deconvoluted high-resolution N 1 s XPS spectra of phytocat display peaks located at 399.1, 399.7, 400.7, and 402.3 eV (Fig. 3b) attributed to pyridinic N, pyrrolic N, graphitic N, and oxidized N, respectively [41]. The shift in the position of the pyrrolic N peak to a higher value for the higher Ni loadings, could be due to charge transfer between Ni and pyrrolic N species [41].

Deconvoluted high-resolution C 1 s XPS spectra of phytocat show characteristics peaks for C–C (284.6 eV), C–N (285.4 eV), C–O

(286.3 eV), C═O (287.2 eV), and O–C═O (288.9 eV) bonds [41]. The prominent peaks at 284.3–284.5 eV reveal that the most carbons in the phytocat are aromatic. The presence of these functional groups on the surface of phytocat facilitates its binding with nickel nano-particles (Fig. 3c). The peaks corresponding to π–π * transition (290.4 eV) were found to intensify for the recycled phytocat.

The O 1 s spectra of phytocat catalysts (Fig. 3d) all comprised three peaks, among which are peaks at 530–531 eV corresponding to the lattice oxygen involved in the metal framework oxide (Ni–O) while the peaks at 531.7–532.9 eV are assigned to oxygen atoms bonded to carbon atoms (C═O bond), and the peaks at higher binding energy of 533.2–534.6 eV are attributed to the chemisorbed oxygen species from C–O in carbonates (CO_3^{2-}) [41]. The peaks corresponding to the carbonates became more prominent in the recycled catalysts.

To understand the crystal structure and phase purity of the phytocat material, X-ray diffraction (XRD) was used. Initial x-ray powder diffraction (XRD) analysis revealed metallic nickel particles along with a carbon rich phase. As shown in Fig.3e, the diffraction peaks at 44.6°, 52.2°, and 77.3° belong to metallic Ni ([111], [200] and [220] diffraction peaks of Ni^0) [42]. Both the phytocat materials exhibits a

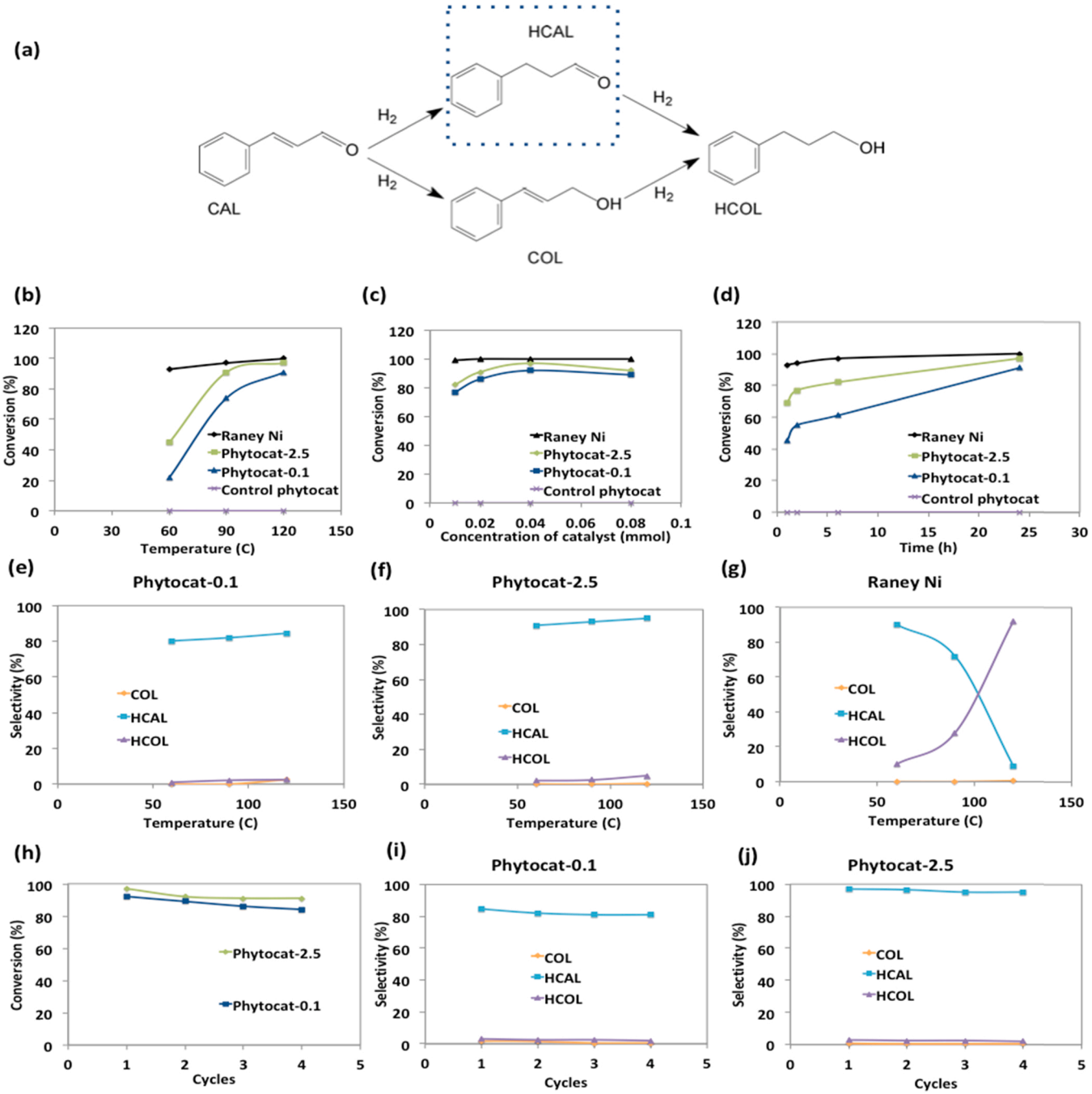

Fig. 4. (a) Mechanistic pathway of hydrogenation of cinnamaldehyde, (b) influence of reaction temperature on the catalytic conversion of cinnamaldehyde, (c) influence of catalyst concentration on the catalytic conversion of cinnamaldehyde, (d) influence of reaction time on the catalytic conversion of cinnamaldehyde, (e) influence of reaction temperature on the product selectivity using phytocat-0.1, (f) influence of reaction temperature on the product selectivity using phytocat-2.5, (g) influence of reaction temperature on the product selectivity using Raney Ni, (h) Reusability of Ni-phytocat for catalytic conversion of cinnamaldehyde, (i) Reusability of Ni-phytocat-0.1 for selectivity towards HCAL, (j) Reusability of Ni-phytocat-2.5 for selectivity towards HCAL. Reaction conditions: 1 mmol substrate, 10–50 mg catalyst (0.01–0.04 mmol Ni), 1–24 h, 5 mL isopropanol, 40 bar H_2, 60–120 °C.

broad graphitic (002) peak at about 25°, which belongs to the hexagonal conjugated carbon structure. This confirms that the structure of the phytocat is relatively stable compared to Raney Ni and the majority of entrapped NiO is reduced to Ni metal by the surrounding bio-carbon matrix during the microwave-assisted pyrolysis. Similarly, after use, the characteristic peaks of bio-carbon ($2\theta = 24.5°$) and Ni metal ($2\theta = 44.5°$, 51.9° and 76.9°) are observed for all the phytocat materials, in which the intensity of [111], [200] and [220] diffraction peaks due to Ni^0 is gradually increased with increasing Ni content (Fig. 3f) [43]. The average size of the Ni nanoparticles using the Scherrer method for the (111) peak was calculated to be 6.5 ± 1.1 nm which is comparable with the results from the TEM analysis. After reuse, the catalyst was recovered and analyzed, and the average particle size was found to be 7.2 ± 1.9 nm using TEM analysis and 7.9 ± 2.1 nm using the Scherrer method.

The Brunauer-Emmett-Teller (BET) surface area of Ni-phytocat-2.5 and Ni-phytocat 0.1 was found to be 34.2 m^2/g and 21.7 m^2/g respectively and contain micro-pores and meso-pores (Fig. S6) [43]. Thermogravimetric analysis (TGA) experiments were conducted to understand the thermal degradation profiles of the raw plant biomass of *S. viminalis* and *A. murale* and also for the prepared phytocat using these materials.

As shown in Supplementary Fig. 5, the raw biomass exhibits an initial weight loss around 370 °C. The TGA plots of Ni-phytocat-2.5, Ni-phytocat-0.1 and control phytocat, prepared using low-temperature microwave activation, indicate a slight weight loss of about 6.1%, 7.2% and 7.5% at low temperature (T≤150 °C), which may be assigned to the removal of the adsorbed water or residual solvents from the surface. This reveals the remarkable thermal stability of phytocat even at high temperatures (T≤700 °C). There are numerous advantages of using microwave-heating, which promotes high dispersion of Ni species, easy reduction of surface Ni species, and formation of uniformly nano-sized Ni particles [44]. Our clean strategy of using simple, one step, low-temperature microwave assisted pyrolysis resulted in the formation of an air stable nickel phytocat, which would be tested further for hydrogenation of a model renewable platform molecule (cinnamaldehyde).

3.2. Tuning reaction conditions to explore the potential of bio-derived Ni catalyst for hydrogenation of a model renewable platform molecule

After establishing the structural features of Ni-phytocat, their catalytic performance was evaluated. Selective hydrogenation of a CAL entails reduction of different functional groups, that is, a carbonyl group (C═O) or a carbon–carbon double bond (C═C) to give the corresponding products cinnamyl alcohol (COL) or hydrocinnamaldehyde (HCAL) (Fig. 4a). Based on thermodynamic and kinetic theory, hydrogenation of the C═C bond is more favorable due to lower bond energy of the C═C group (615 kJ/mol) [27,45]. It is vital to improve the selectivity to a certain group (C═O or C═C bond) and to avoid the hydrogenation of another one. Selectivity can be correlated with a metal d-bandwidth, and a smaller radial expansion of the d orbitals, leading to higher selectivity to HCAL [18,35]. Thus, some metals with a relatively large d-bandwidth (i.e. Ru, Ir and Pt) can be used as catalysts to synthesize COL, while the ones with small d-bandwidth (like Ni) favored HCAL [18,35]. The nature of adsorption and desorption of reactants (CAL) is governed by the changes in catalyst compositions, electronic structure, chemical state, and morphology of metal and supports, thereby determining the selectivity and yield of different products i.e. COL, HCAL or hydrocinnamyl alcohol (HCOL) [22,46]. One of the main approaches to catalyst design to enhance catalytic performance is to tune the metal–metal oxide interactions in the catalyst, which could lead to charge transfer between the metal and support [22,46].

To showcase the activity and selectivity of Ni-phytocat, its activity was compared with Raney Ni. The hydrogenation of CAL afforded HCAL from C═C hydrogenation and HCOL from complete hydrogenation (C═C and C═O reduction). The control phytocat (pristine bio-carbon, <0.01 wt% Ni) was also tested. Phytocat-2.5 exhibited a high activity (up to 97% CAL conversion and 96% HCAL selectivity) as compared with phytocat-0.1 (up to 89% CAL conversion and 87% HCAL selectivity). In comparison to phytocat-2.5 and 0.1, negligible activity was observed using the control phytocat, while Raney Ni exhibited excellent activity (up to 99.9% CAL conversion) but lower selectivity (up to 82% HCAL selectivity). Because C═C hydrogenation is thermodynamically favored, Ni-based catalysts prefer C═C hydrogenation and HCAL generation [27,35]. Although Raney Ni is non-selective towards the desired product, it works well under mild reaction conditions (40 bar H_2, 60 °C). In order to optimize the conversion of CAL and the selectivity to HCAL, some factors influencing the reaction such as reaction temperature, reaction time and concentration of catalysts were explored.

3.2.1. Influence of reaction temperature on catalytic hydrogenation of cinnamaldehyde

The influence of reaction temperature on the hydrogenation of CAL to HCAL was investigated in the range of 60–120 °C (Fig. 4b). Increasing the hydrogenation temperature favored the conversion of CAL, which increased from 22% (60 °C) to 89% (120 °C), 43% (60 °C) to 97% (120 °C) and 94 (60 °C) to 99.9% (120 °C) for phytocat-0.1, phytocat-2.5 and Raney Ni respectively. As the temperature continued to increase, the selectivity to HCAL increased to 84%, 97% and 97.5%, respectively at 120 °C. Thus, 120 °C was chosen as the optimum reaction temperature. As listed in Supplementary Table 2, when Ni-based catalysts were applied, a higher reaction temperature and H_2 pressure were required, as compared to that when noble metal catalysts were used, due to the relatively low activity of Ni [15,34]. It is essential that the activity of Ni-based catalysts is further improved through novel structure design. Many researchers have used synthetic catalysts such as Ni supported on reduced graphene oxide (RGO) or Ni supported on activated carbon at high temperatures (T > 150 °C) and achieved up to 91% CAL conversion with upto 82% HCAL [34,47].

3.2.2. Influence of concentration of catalysts on selective hydrogenation of cinnamaldehyde

Several reports revealed that preparation methods affected the Ni crystal size and the nature of metal–support interactions and, thereby, influenced the activity of the catalysts [46,38,40]. After studying the structural characteristics of the phytocat materials, it is clear that the phytocat-2.5 has highly dispersed catalytically active Ni^0 sites. Due to the presence of highly dispersed and uniformly nano-sized Ni particles, phytocat-2.5 showed superior catalytic performance. With increasing catalyst concentration, there was an increase in CAL conversion, leading to creation of the target product (97% and 89% HCAL) using phytocat-2.5 and 0.1 respectively (Fig. 4c). Although Raney Ni is non-selective towards the HCAL, it worked well even at lower concentrations (0.01 mmol) and showed a stable reaction profile throughout (Fig. 4c and Fig. S8a Fig. S6a).

3.2.3. Influence of reaction time on catalytic hydrogenation of cinnamaldehyde

Fig. 4d shows the variability of the conversion and selectivity with changing reaction time (1–24 h) at constant reaction temperature of 120 °C. The conversion grew sharply by 45–84%, 77–97% and 94–99.9% with phytocat-0.1, phytocat-2.5 and Raney Ni respectively, when the reaction time was extended from 1 h to 24 h. With the change of reaction time, the selectivity remained stable at about 95% and reached the maximum of 96.5% at 2 h (Fig. S8b). This alludes to the difficulty of C═O bond reduction [48]. As the reaction time is prolonged to above 6 h, the selectivity to HCAL is slightly decreased to 93.9%. As shown in Supplementary Table 2, the NiAl-LDH/G (Ni–Al layered double hydroxide/graphene) and Ni-Cu@RGO (RGO: reduced graphene oxide) catalysts showed high activity and high selectivity to HCAL as well [34,49]. Despite the high activity of Ni-Cu@RGO, its fabrication

was done using a synthetic route and the catalytic performance was tested at high temperature (T > 150 °C) [34].

3.2.4. Catalyst stability

Reusability is an important catalyst performance indicator and was therefore investigated here (Fig. 4h-j). We performed the reusability tests using phytocat-0.1 and phytocat-2.5 to illustrate their stability and performance for four cycles. The catalyst was recovered, washed with isopropanol three times and dried overnight. The catalyst was then weighed and transferred in a stainless steel multipoint (6 × 10 mL pots) reactor (manufactured at chemistry workshops, University of York). Following the same procedures, the reaction was carried out at 120 °C and pressurized to 40 bar H_2. The sampling was done after 24 h of reaction, and the catalyst was recycled four times. Notably, after the third cycle, the conversion of CAL remained at 96% with 94% chemoselectivity (Fig. 4h-j), as demonstrated by Fourier transform infrared spectroscopy (FT-IR) analysis of the products formed after catalytic hydrogenation of cinnamaldehyde using pristine and recycled phytocat-0.1 and phytocat-2.5 (Fig. S11-S12). For the first to the third catalytic cycles we achieved conversions of > 94%; a decrease in conversion was observed in the fourth catalytic run due to the mass lost during recycling and possibly due to deactivation of the catalyst (Fig. 4h). The structural integrity of the catalyst remained intact after as many as four catalytic cycles. The high-angle annular dark-field scanning transmission electron microscopy (HAADF-STEM) image of the recycled catalyst shows structural features that are the same as the pristine catalyst (Fig. S1). The shape and the sizes of the NPs are comparable to the pristine catalysts (6.1±1.1 nm). These Ni NPs contained within the bio-carbon matrix of phytocat possess good thermal stability because of the constraints of the carbon support, which limit its aggregation and leads to excellent catalytic activity. The well-maintained catalytic performance after four-consecutive runs demonstrates a high stability and reusability of Ni-phytocat. This can be attributed to the superior structural stability of Ni-phytocat as evidenced by the almost unchanged structure, morphology, crystal phase and chemical forms of the reused Ni-phytocat (Fig. 3; Fig.S1).

To further illustrate the role of **the** bio-carbon matrix around the phyto-extracted Ni, which enables an efficient suppression of the over-hydrogenation reaction pathway and prevents further dissociation of adsorbed hydrocinnamaldehyde molecules, we performed catalytic hydrogenation tests on furfural and levoglucosenone (LGO) (Fig. S20, 21). Based on the results, we found that the control phytocat (pristine bio-carbon matrix) was ineffective in all the hydrogenation tests even after long reaction times (24 h) and high temperature (120℃). In contrast, our Ni-phytocat was successful in converting LGO into dihydrolevoglucosenone (Cyrene™, up to 81% conversion), while it was unable to convert furfural into furfuryl alcohol. While with Raney Ni, we observed the formation of levoglucosanol (Lgol) instead of Cyrene™. These findings clearly demonstrate that the presence of the bio-carbon matrix around our Ni-phytocat enables an efficient suppression of the over-hydrogenation reaction pathway, making it highly selective towards the formation of saturated aldehydes over alcohols. Our Ni-phytocat selectively prefers the hydrogenation of C═C bonds over C═O bonds, resulting in the formation of the corresponding saturated aldehyde rather than the unsaturated alcohol.

4. Conclusions

A biologically bound non-noble metal catalyst (low metallic loadings: 0.1–2.5 wt% Ni) was prepared using a simple, one-step, energy efficient, low temperature, microwave-assisted pyrolysis (250℃, 200 W, <10 min). The Ni-based biocatalyst (phytocat) represents a hybrid platform consisting of naturally occurring, inorganic components with lignocellulose providing an exciting opportunity to advance green chemistry applications. Most importantly, the biologically bound Ni in the plant matrix directs the catalytic hydrogenation of cinnamaldehyde (up to 97% conversion at T≤ 120℃), thereby removing the need for traditionally mined metal. Most of the reported work on the partial reduction of cinnamaldehyde (CAL) shows either poor selectivity (<13%) or poor conversion (<63%) [20,47]. Moreover, there remain challenges associated with the overall sustainability of the transformation i.e. relatively high cost or complex synthetic protocol for fabrication of catalyst or high reaction temperatures (T > 150℃) [34, 47]. HCAL and its derivatives have established themselves as industrially and biologically valuable in the synthesis of natural products, anti-viral pharmaceuticals, fragrances and chemosensors [29,28,50,51]. Our findings indicate that the presence of bio-carbon matrix around the naturally entrapped Ni enables an efficient suppression of the over-hydrogenation reaction pathway and carbonaceous accumulation on the surface. That is, the natural encapsulation of nickel on bio-carbon not only inhibits the unselective hydrogenation pathway but also regulates the electronic structure of Ni. Therefore, it suppresses the further dissociation of adsorbed hydrocinnamaldehyde (HCAL) molecules, leading to its high selectivity (up to 96%) at low temperatures (T≤ 120℃). The overall sustainability and stability of Ni-phytocat is significantly higher in comparison with traditional synthetic catalysts.

CRediT authorship contribution statement

Parul Johar: Conceptualization, Investigation, Analysis, Writing – original draft, Writing – review & editing, Resources, Funding acquisition. **C. Robert Mc.Elroy**: Resources, Supervision, Writing – review & editing. **Elizabeth L. Rylott**: Resources, Supervision, Writing – review & editing. **Avtar S. Matharu**: Supervision, Writing – review & editing. **James H. Clark**: Conceptualization, Supervision, Writing – review & editing, Resources, Funding acquisition.

Declaration of Competing Interest

The authors declare that they have no known competing financial interests or personal relationships that could have appeared to influence the work reported in this paper.

Acknowledgements

The authors acknowledge the financial support from the University of York (Wild Fund Platinum Scholarship). We also acknowledge the assistance of Dr. Baptiste Laubie and Dr. Guillaume Echevarria from University of Lorraine in the field collection of hyper- accumulator species. We are grateful to receive the technical support from Mr. Karl Heaton, Dr. Jon Barnard and Dr. Leonardo Lari.

Appendix A. Supporting information

Supplementary data associated with this article can be found in the online version at doi:10.1016/j.apcatb.2022.121105.

References

[1] L.J. Sonter, M.C. Dade, J.E.M. Watson, R.K. Valenta, Renewable energy production will exacerbate mining threats to biodiversity, Nat. Commun. 11 (2020) 4174, https://doi.org/10.1038/s41467-020-17928-5.
[2] Mineral commodity summaries 2020, Reston, VA, 2020. https://doi.org/10.3133/mcs2020.
[3] G. Tóth, T. Hermann, M.R. Da Silva, L. Montanarella, Heavy metals in agricultural soils of the European Union with implications for food safety, Environ. Int. 88 (2016) 299–309, https://doi.org/10.1016/j.envint.2015.12.017.
[4] L. Wang, D. Hou, Z. Shen, J. Zhu, X. Jia, Y.S. Ok, F.M.G. Tack, J. Rinklebe, Field trials of phytomining and phytoremediation: a critical review of influencing factors and effects of additives, Crit. Rev. Environ. Sci. Technol. 50 (2020) 2724–2774.
[5] J. Luo, S. Qi, X.W.S. Gu, J. Wang, X. Xie, Evaluation of the phytoremediation effect and environmental risk in remediation processes under different cultivation systems, J. Clean. Prod. 119 (2016) 25–31.
[6] D. Tőzsér, S. Harangi, E. Baranyai, G. Lakatos, Z. Fülöp, B. Tóthmérész, E. Simon, Phytoextraction with Salix viminalis in a moderately to strongly contaminated area, Environ. Sci. Pollut. Res. 25 (2018) 3275–3290.

[7] B.-H. Cheng, B.-C. Huang, R. Zhang, Y.-L. Chen, S.-F. Jiang, Y. Lu, X.-S. Zhang, H. Jiang, H.-Q. Yu, Bio-coal: a renewable and massively producible fuel from lignocellulosic biomass, Sci. Adv. 6 (2020), https://doi.org/10.1126/sciadv.aay0748.

[8] R.A.J. W.C. K, D.B. H, B. George, C. John, E.C. A, F.W.J. H.J. P, L.D.J. L.C. L, M.J. R, M. Richard, T. Richard, T. Timothy, The path forward for biofuels and biomaterials, Science 311 (2006) 484–489, https://doi.org/10.1126/science.1114736.

[9] C.J.M. C.A. M, G. Ramon, Industrial biomanufacturing: the future of chemical production, Science 355 (2017) aag0804, https://doi.org/10.1126/science.aag0804.

[10] R.P. Lopes, D. Astruc, Biochar as a support for nanocatalysts and other reagents: recent advances and applications, Coord. Chem. Rev. 426 (2021), 213585.

[11] S. Sadjadi, M. Akbari, B. Léger, E. Monflier, M.M. Heravi, Eggplant-derived biochar-halloysite nanocomposite as supports of Pd nanoparticles for the catalytic hydrogenation of nitroarenes in the presence of cyclodextrin, ACS Sustain. Chem. Eng. 7 (2019) 6720–6731.

[12] X. Lu, J. He, R. Jing, P. Tao, R. Nie, D. Zhou, Q. Xia, Microwave-activated Ni/carbon catalysts for highly selective hydrogenation of nitrobenzene to cyclohexylamine, Sci. Rep. 7 (2017) 2676, https://doi.org/10.1038/s41598-017-02519-0.

[13] Z. Tao, Taking on all of the biomass for conversion, Science 367 (2020) 1305–1306, https://doi.org/10.1126/science.abb1463.

[14] L. Ceatra, O.C. Pârvulescu, I. Rodríguez Ramos, T. Dobre, Preparation, characterization, and testing of a carbon-supported catalyst obtained by slow pyrolysis of nickel salt impregnated vegetal material, Ind. Eng. Chem. Res. 55 (2016) 1491–1502, https://doi.org/10.1021/acs.iecr.5b04059.

[15] S. Gryglewicz, A. Śliwak, J. Ćwikła, G. Gryglewicz, Performance of carbon nanofiber and activated carbon supported nickel catalysts for liquid-phase hydrogenation of cinnamaldehyde into hydrocinnamaldehyde, Catal. Lett. 144 (2014) 62–69.

[16] R. Bardestani, R. Biriaei, S. Kaliaguine, Hydrogenation of furfural to furfuryl alcohol over Ru particles supported on mildly oxidized biochar, Catalysts 10 (2020) 934.

[17] H. Xin, W. Zhang, X. Xiao, L. Chen, P. Wu, X. Li, Selective hydrogenation of cinnamaldehyde with NixFe1-xAl2O4+ δ composite oxides supported Pt catalysts: CO versus CC selectivity switch by varying the Ni/Fe molar ratios, J. Catal. 393 (2021) 126–139.

[18] A. Egeberg, C. Dietrich, C. Kind, R. Popescu, D. Gerthsen, S. Behrens, C. Feldmann, Bimetallic nickel-iridium and nickel-osmium alloy nanoparticles and their catalytic performance in hydrogenation reactions, ChemCatChem 9 (2017) 3534–3543.

[19] M. Raney, Method for producing Finely Divided Nickel, US Pat., 1628190, Issued 1927-05-10, 1927.

[20] M.G. Prakash, R. Mahalakshmy, K.R. Krishnamurthy, B. Viswanathan, Studies on Ni–M (M= Cu, Ag, Au) bimetallic catalysts for selective hydrogenation of cinnamaldehyde, Catal. Today 263 (2016) 105–111.

[21] R. Murray, Method of preparing catalytic material (1925).

[22] Y. Niu, X. Huang, Y. Wang, M. Xu, J. Chen, S. Xu, M.-G. Willinger, W. Zhang, M. Wei, B. Zhang, Manipulating interstitial carbon atoms in the nickel octahedral site for highly efficient hydrogenation of alkyne, Nat. Commun. 11 (2020) 3324, https://doi.org/10.1038/s41467-020-17188-3.

[23] C. Li, G. Xu, Y. Zhai, X. Liu, Y. Ma, Y. Zhang, Hydrogenation of biomass-derived ethyl levulinate into Γ-valerolactone by activated carbon supported bimetallic Ni and Fe catalysts, Fuel 203 (2017) 23–31, https://doi.org/10.1016/j.fuel.2017.04.082.

[24] D. Verma, R. Insyani, H.S. Cahyadi, J. Park, S.M. Kim, J.M. Cho, J.W. Bae, J. Kim, Ga-doped Cu/H-nanozeolite-Y catalyst for selective hydrogenation and hydrodeoxygenation of lignin-derived chemicals, Green Chem. 20 (2018) 3253–3270, https://doi.org/10.1039/C8GC00629F.

[25] M. Zhao, K. Yuan, Y. Wang, G. Li, J. Guo, L. Gu, W. Hu, H. Zhao, Z. Tang, Metal–organic frameworks as selectivity regulators for hydrogenation reactions, Nature 539 (2016) 76–80.

[26] X. Wang, X. Liang, P. Geng, Q. Li, Recent advances in selective hydrogenation of cinnamaldehyde over supported metal-based catalysts, ACS Catal. 10 (2020) 2395–2412.

[27] P. Gallezot, D. Richard, Selective hydrogenation of α, β-unsaturated aldehydes, Catal. Rev. 40 (1998) 81–126.

[28] D. Pybus, C. Sell, The Chemistry of Fragrances, The Royal Society of Chemistry, 2006, https://doi.org/10.1039/9781847555342.

[29] A.M.C.F. Castelijns, J.M. Hogeweg, S.P.J.M. Van Nispen, Process for the preparation of 3-phenylpropanal (1998).

[30] D.T. Payne, Y. Zhao, J.S. Fossey, Ethylenation of aldehydes to 3-propanal, propanol and propanoic acid derivatives, Sci. Rep. 7 (2017) 1720, https://doi.org/10.1038/s41598-017-01950-7.

[31] C.G. Frost, B.C. Hartley, Tandem molybdenum catalyzed hydrosilylations: an expedient synthesis of β-aryl aldehydes, Org. Lett. 9 (2007) 4259–4261, https://doi.org/10.1021/ol701812w.

[32] C.G. Frost, B.C. Hartley, Lewis base-promoted hydrosilylation of cyclic malonates: synthesis of β-substituted aldehydes and γ-substituted amines, J. Org. Chem. 74 (2009) 3599–3602, https://doi.org/10.1021/jo900390d.

[33] H. Wang, Y. Shi, Z. Wang, Y. Song, M. Shen, B. Guo, L. Wu, Selective hydrogenation of cinnamaldehyde to hydrocinnamaldehyde over Au-Pd/ultrathin SnNb2O6 nanosheets under visible light, J. Catal. 396 (2021) 374–386.

[34] S.S. Mohire, G.D. Yadav, Selective synthesis of hydrocinnamaldehyde over bimetallic Ni–Cu nanocatalyst supported on graphene oxide, Ind. Eng. Chem. Res. 57 (2018) 9083–9093.

[35] S. Padmanaban, G.H. Gunasekar, S. Yoon, Direct heterogenization of the Ru-macho catalyst for the chemoselective hydrogenation of α, β-unsaturated carbonyl compounds, Inorg. Chem. 60 (2021) 6881–6888.

[36] P. Johar, E.L. Rylott, C.R. McElroy, A.S. Matharu, J.H. Clark, Phytocat – a bio-derived Ni catalyst for rapid de-polymerization of polystyrene using a synergistic approach, Green Chem. 23 (2021) 808–814, https://doi.org/10.1039/D0GC03808C.

[37] A. van der Ent, D.L. Callahan, B.N. Noller, J. Mesjasz-Przybylowicz, W. J. Przybylowicz, A. Barnabas, H.H. Harris, Nickel biopathways in tropical nickel hyperaccumulating trees from Sabah (Malaysia), Sci. Rep. 7 (2017) 41861, https://doi.org/10.1038/srep41861.

[38] H. Yang, Q. Lin, C. Zhang, X. Yu, Z. Cheng, G. Li, Q. Hu, X. Ren, Q. Zhang, J. Liu, Carbon dioxide electroreduction on single-atom nickel decorated carbon membranes with industry compatible current densities, Nat. Commun. 11 (2020) 1–8.

[39] G.W. Brindley, D.L. Bish, H.-M. Wan, Compositions, structures, and properties of nickel-containing minerals in the kerolite-pimelite series, Am. Mineral. 64 (1979) 615–625.

[40] B.H. Lipshutz, Development of nickel-on-charcoal as a "'dirt-cheap"' heterogeneous catalyst: a personal account, Adv. Synth. Catal. 343 (2001) 313–326, https://doi.org/10.1002/1615-4169(20010430)343:4<313::AID-ADSC313>3.0.CO;2-A.

[41] C.J. Powell, Elemental binding energies for X-ray photoelectron spectroscopy, Appl. Surf. Sci. 89 (1995) 141–149.

[42] W. ~H. Qi, M. ~P. Wang, Size and shape dependent lattice parameters of metallic nanoparticles, J. Nanopart. Res. 7 (2005) 51–57, https://doi.org/10.1007/s11051-004-7771-9.

[43] R.G. Nuzzo, L.H. Dubois, N.E. Bowles, M.A. Trecoske, Derivatized, high surface area, supported nickel catalysts, J. Catal. 85 (1984) 267–271.

[44] J. Lin, S. Sun, D. Xu, C. Cui, R. Ma, J. Luo, L. Fang, H. Li, Microwave directional pyrolysis and heat transfer mechanisms based on multiphysics field stimulation: design porous biochar structure via controlling hotspots formation, Chem. Eng. J. (2021), 132195.

[45] B. Bachiller-Baeza, I. Rodrıguez-Ramos, A. Guerrero-Ruiz, Influence of Mg and Ce addition to ruthenium based catalysts used in the selective hydrogenation of α, β-unsaturated aldehydes, Appl. Catal. A Gen. 205 (2001) 227–237.

[46] B. Li, H.C. Zeng, Formation combined with intercalation of Ni and its alloy nanoparticles within mesoporous silica for robust catalytic reactions, ACS Appl. Mater. Interfaces 10 (2018) 29435–29447.

[47] L.J. Malobela, J. Heveling, W.G. Augustyn, L.M. Cele, Nickel–Cobalt on carbonaceous supports for the selective catalytic hydrogenation of cinnamaldehyde, Ind. Eng. Chem. Res. 53 (2014) 13910–13919.

[48] A. Zhou, Y. Dou, J. Zhou, J.-R. Li, Rational localization of metal nanoparticles in yolk–shell MOFs for enhancing catalytic performance in selective hydrogenation of cinnamaldehyde, ChemSusChem 13 (2020) 205–211.

[49] M.Y. Miao, J.T. Feng, Q. Jin, Y.F. He, Y.N. Liu, Y.Y. Du, N. Zhang, D.Q. Li, Hybrid Ni–Al layered double hydroxide/graphene composite supported gold nanoparticles for aerobic selective oxidation of benzyl alcohol, RSC Adv. 5 (2015) 36066–36074.

[50] J.S. Yadav, P.A.N. Reddy, A.S. Kumar, A.R. Prasad, B.V.S. Reddy, A.A.Al Ghamdi, Stereoselective total synthesis of 4-((3S,5R)-3,5-dihydroxynonadecyl)phenol, Tetrahedron Lett. 55 (2014) 1395–1397, https://doi.org/10.1016/j.tetlet.2013.12.056.

[51] W. Chen, S.A. Elfeky, Y. Nonne, L. Male, K. Ahmed, C. Amiable, P. Axe, S. Yamada, T.D. James, S.D. Bull, J.S. Fossey, A pyridinium cation–π interaction sensor for the fluorescent detection of alkyl halides, Chem. Commun. 47 (2011) 253–255, https://doi.org/10.1039/C0CC01420F.